A Platinum Open Access Journal for Organic Chemistry

Paper

Free to Authors and Readers | DOAJ Seal | *Arkivoc* **2021**, part viii, 63-76

Isolation and structural characterization of novel thermal degradation impurity of nafcillin sodium using spectroscopic and computational techniques

Prasad Yaragorla,[a] Yesudas Kada,[a] Krishnam Raju Ch,[b] Arunima Pola,[b] Rabin Bera,[a*] and Sanath Kumar Goud P[b]

[a]Synthetic Laboratory and [b]Analytical Research and Development, United States Pharmacopeial Convention – India (P) Ltd., Hyderabad-500101, India

Email: rxb@usp.org

Received 11-18-2020 **Accepted Manuscript** 02-05-2021 **Published on line** 02-18-2021

Abstract

Thermal degradation of nafcillin sodium (**NS**) gave rise to an unknown impurity. This unknown thermal degradation impurity (**TDI**) was evaluated using a reverse-phase high performance liquid chromatography, where it was eluted at 1.31 relative retention time to **NS** peak. **TDI** was isolated using preparative HPLC from degradation mixture and fully characterized using the various spectroscopic techniques like high resolution MS, multidimensional NMR and FTIR. Based on the available spectroscopic data, the probable structure for the impurity is proposed and is named as (2R,4S)-2-((R)-carboxy(2-ethoxy-1-naphthamido)methyl)-3-((2-ethoxy-1-naphthoyl)glycyl)-5,5-dimethylthiazolidine-4-carboxylic acid. The proposed structure is further supported by the density functional theory calculations. In addition, a two-step mechanism of the degradation is proposed. To the best of our knowledge, it is a novel impurity and not reported elsewhere.

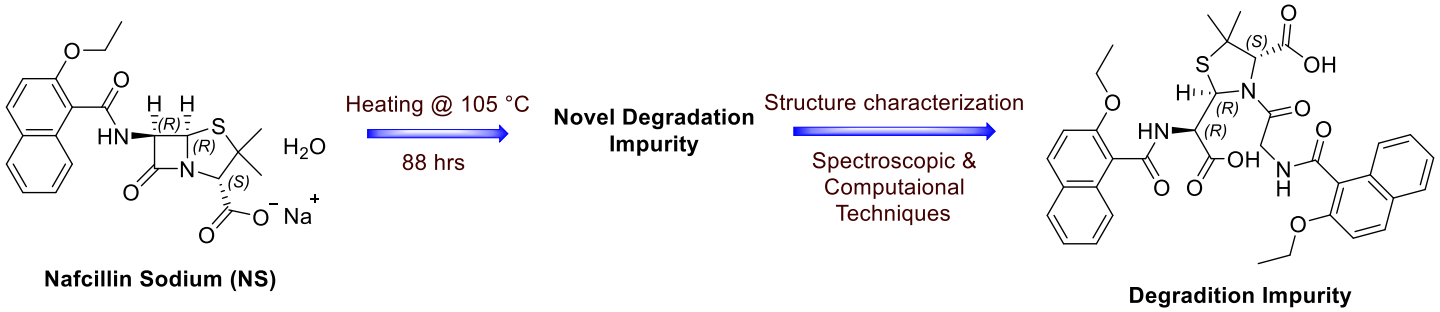

Keywords: Novel impurity of nafcillin sodium, degradation, HPLC, NMR, HRMS, computational chemistry

Introduction

Nafcillin sodium (**NS**) is a parenteral, second generation penicillinase-resistant penicillin antibiotic used largely to treat moderate to severe staphylococcal infections. It is a semi-synthetic naphthalene, beta-lactam antibiotic and the chemical structure is shown in Figure 1. These semi-synthetic agents are engineered to be resistant to hydrolysis by most staphylococcal β-lactamases by virtue of a substituted side chain that acts by steric hindrance at the site of enzyme attachment.[1] Its bactericidal activity is triggered by inhibition of bacterial cell wall synthesis by forming covalent bond to one or more of the penicillin binding proteins that play a critical role in the final transpeptidation process. Binding to penicillin-binding proteins inhibits the transpeptidase and carboxypeptidase activities conferred by these proteins and prevents the formation of the crosslinks.[2] This has been linked to rare occurrences of clinically apparent, idiosyncratic liver injury.[3] It is administrated orally and by intramuscular and intravenous injections. However, it is poorly absorbed after oral administration, and absorption is further depressed if the drug is given with food. The levels are low even if administered by intramuscular injection. Therefore, most dosing is now intravenous.[4]

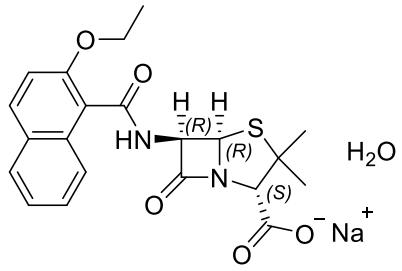

Nafcillin Sodium (NS)

Figure 1. Chemical structure of nafcillin sodium (**NS**).

To have a benchmark quality of the drug substance and to meet various guidelines such as International Conference on Harmonization (ICH) and regulatory requirements, it is important to identify the impurities present in the drug substance.[5, 6] The requirement of stability testing data is to understand how the quality of a drug substance and drug product changes with time under the influence of various environmental factors.[5, 6] This indeed helps in selecting proper formulation and package as well as providing proper storage conditions and shelf life.[7] To this end, Prasada Rao *et. al.* reported the formation of various degradation impurities of **NS** during the stress and formal stability storage conditions as per ICH requirements.[8] Ashline *et. al.* has reported a novel thietan-2-one degradation impurity in aqueous solution[9] while Jagadeesh *et. al.* has reported a new degradation impurity under thermal and humidity condition.[10]

In the present study, **NS** subjected to degradation under thermal conditions. The HPLC chromatogram of **NS** showed the formation of an unknown impurity along with four known impurities at the relative retention time (RRT) of around 1.31 with respect to **NS** peak. The four known impurities obtained at RRT of ~0.49 (14.10 %), ~0.67 (12.05%), and ~0.84 (8.23 %) are found to be Penicilloic acid of Nafcillin, Penilloic acids of Nafcillin-1 and 2 and 2-ethoxy-1-napthoic acid respectively as reported by Prasada Rao *et.al*.[8] Here we present in detail the identification, isolation, structure elucidation and the mechanism of formation of this unknown thermal degradation impurity (**TDI**).

Results and Discussion

Characterization of TDI

Mass structural characterization studies

LC–MS analysis indicated the presence of protonated ions $[M+H]^+$ of **TDI** and **NS** drug substance at m/z 688.42 Da and 415.26 Da respectively. HRMS data indicated that the molecular ions $[M+H]^+$ of **TDI** and $[M+Na]^+$ of **NS** at m/z 688.2343 Da and 437.1152 Da (Table 1). The significant addition of 273.1011 Da in **TDI** against **NS** might be due to the addition of $C_{15}H_{15}NO_4$ (exact mass 273.1001 Da). Molecular formula of protonated **TDI** worked out as $C_{36}H_{38}N_3O_9S^+$, with mass error, 2.0 ppm (exact mass 688.2323 Da). Double bond equivalence (DBE) 19.5 and odd number (three) nitrogen atoms were considered to determine the structure. The chemical structure of **TDI** was investigated thoroughly using HRMS fragmentation and multi-stage mass fragmentation (MS^n) techniques. The obtained data is presented in Table 1 provided the evidence to the proposed chemical structure of **TDI**. The possible structures were proposed for fragments of **TDI** and shown in Figure 2. Molecular ion 688.2343 fragmented to 670.2236 due to the water loss in **TDI**. Molecular ion 688.2343 fragmented to 433.1483 due to the amide bond cleavage at five membered ring. The fragmented ion 433.1483 further fragmented in to 389.1547 with the loss of CO_2. The fragment ions 670.2236 and 389.1547 further fragmented and produced a common fragment ion 199.0770 due to the amide bond cleavage.

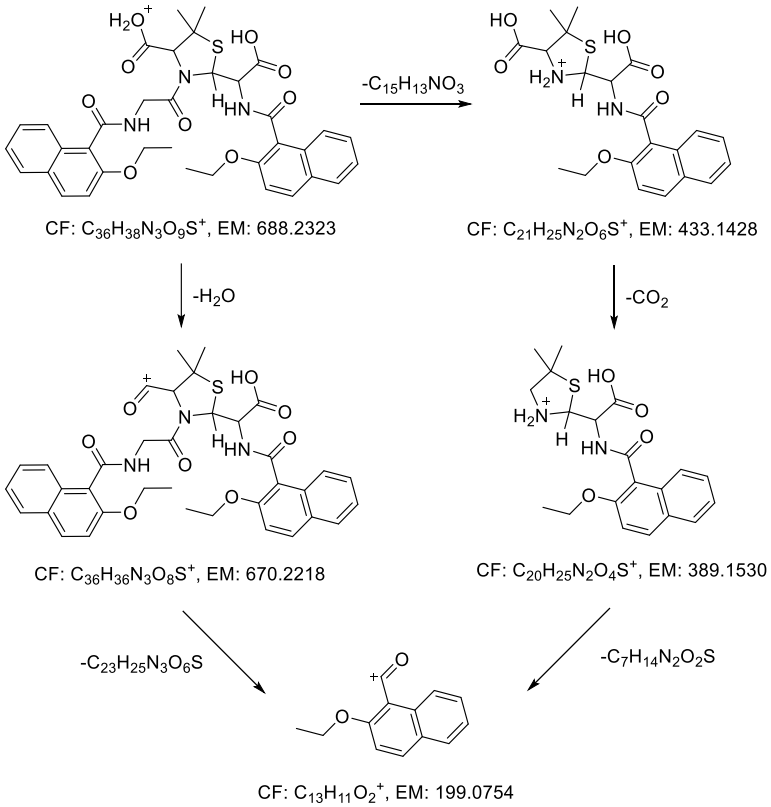

Figure 2. Proposed mass fragments for **TDI (**CF: Chemical formula; EM: Exact mass).

Table 1. HRMS and multi-stage mass fragmentation (MS^n) data of **TDI**

Fragment ion	HRMS data		MS^n data	
	Accurate mass	Accurate masses of fragments	Precursor ion	Product ion(s)
[**TDI** + H]$^+$	688.2343	670.2236, 433.1483, 389.1547, 256.0964, 199.0770, 171.0447	688	670, 433, 389, 199
			688 → 670	199
			688 → 433	389, 199
			688 → 433 → 389	199

NMR structural characterization studies

The values of ^{1}H and ^{13}C NMR chemical shifts (δ) and proton-proton coupling constants (J) of **TDI** are presented in Table 2. ^{1}H and ^{13}C NMR displayed 37 protons and 36 carbons respectively. DEPT90, DEPT135 and ^{13}C NMR experiments verified that **TDI** contains 4–CH_3, 3–CH_2, 15–CH and 14–C carbons. The experimental number of carbons precisely matched with the theoretically calculated number of carbons at proposed chemical structure of **TDI** as shown in Figure 2. Based on the MS^n fragmentation and the NMR data, the proposed chemical structure is shown in Figure 3. Although this impurity is formed at 1.31 RRT which is very close to the impurity reported by Prasad et. al at 1.26 RRT having the chemical structure **TDI-1**[10] as shown in Figure 3, the structure proposed here is entirely different. The major difference between these two structures is that **TDI** has a thiazolidine ring whereas **TDI-1** has an open chain structure. This is evidenced by the NMR data that in **TDI** a doublet signal for proton is observed at 5.85 ppm and 66.02 ppm which correspond to -CH, (sp3 carbon) while in **TDI-1**, a multiplet signal for proton is observed at 7.33 ppm and 161.4 ppm which corresponds to ethylene =CH, (sp2 carbon) at C25. The proposed structure is further supported by notable HMBC correlations between H2/C4, H9/C7, H23&H23'/C19 and H25/C27, Figure 4. HSQC, COSY and TOCSY data was consistent and further supports the proposed chemical structure of **TDI** (refer supplementary material for spectra).

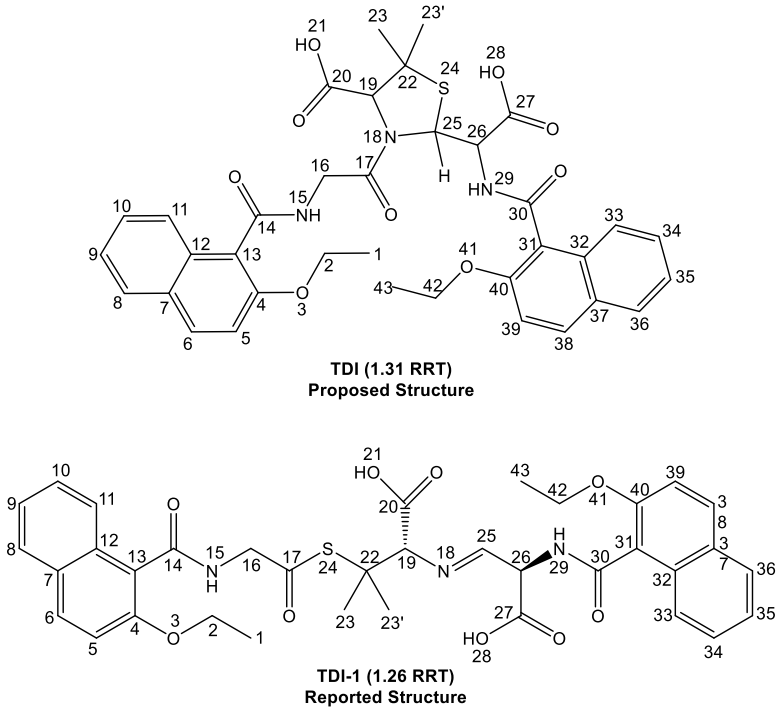

Figure 3. Proposed structure for **TDI** along with the reported structure of **TDI-1** (1.26 RRT).

Table 2. ^{1}H and ^{13}C NMR chemical shifts (δ, ppm) and coupling constants (J, Hz) for **TDI** in DMSO-d_6 at 298 K

Position	δ_H (ppm)	Multiplicity and J(Hz)	DEPT/APT	δ_C (ppm)
1 & 43	1.32	t / 6.9 (3H)	CH_3 (2)	14.86, 14.82
	1.27	t / 6.9 (3H)		
2 & 42	4.16	m (2H)	CH_2 (2)	64.85(2)
	4.14	m (2H)		
4 & 40	-	-	C (2)	152.68, 152.36
5 & 39	7.42	m (1H)	CH (2)	115.37, 115.24
	7.40	m (1H)		
6 & 38	7.94	m (1H)	CH (2)	130.39, 130.12
	7.92	m (1H)		
7, 12, 32 & 37	-	-	C (4)	131.11, 131.03
				128.18, 128.17
8, 11, 33 & 36	7.95, 7.85	m (4H)	CH (4)	127.70,127.59,
				124.76, 124.41
9, 10, 34& 35	7.45, 7.34	m (4H)	CH (4)	126.74(2),
				123.74, 123.68
13 & 31	-	-	C (2)	121.69, 121.01
14	-	-	C	166.80
15	8.40	t / 5.4 (1H)		
16a, 16b	4.23, 4.02	bp (2H)	CH_2	42.47
17	-	-	C	170.26
19	4.81	bp(1H)	CH	72.60
20	-	-	C	170.90
21 & 28	13.21	bp (2H)	-	-
22	-	-	C	50.78
23, 23’	1.70	s (3H)	CH_3 (2)	33.00, 26.02
	1.44	s (3H)		
25	5.85	d / 4.5 (1H)	CH	66.02
26	5.61	bp(1H)	CH	55.45
27	-	-	C	170.58
29	8.05	bp(1H)	-	-
30	-	-	C	166.54

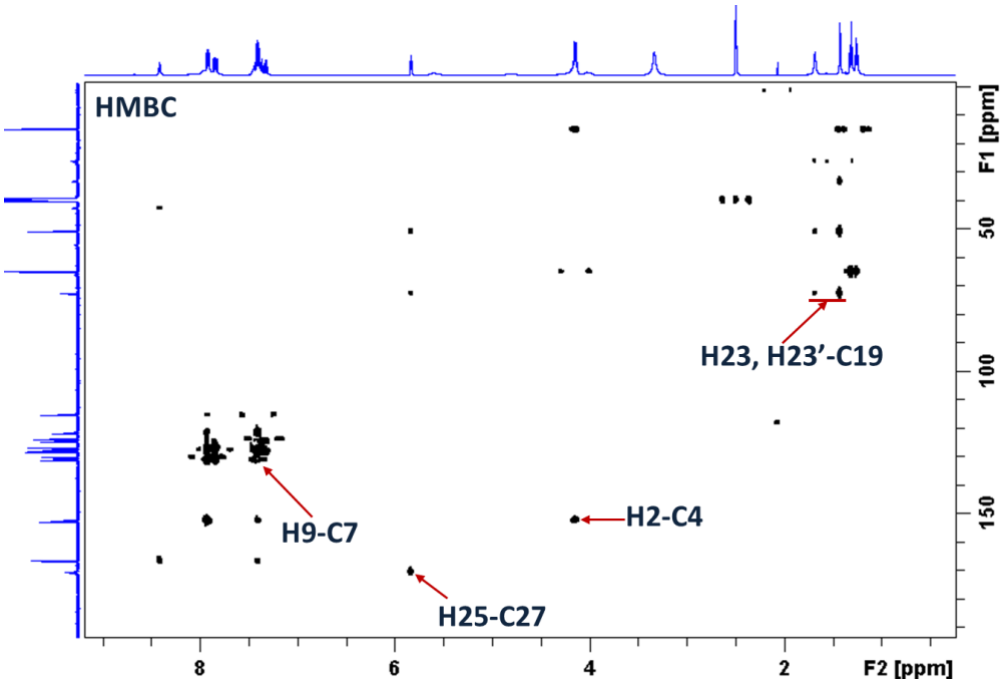

Figure 4. HMBC Spectra for **TDI**.

Structure confirmation by Computational NMR

To support further the proposed structure of **TDI** and to show the differences between the **TDI** and **TDI-1** as shown in Figure 3, both the ^{1}H and ^{13}C NMR chemical shift values were predicted using the computational techniques. The geometries of both the structures were fully energy minimized at the same level as discussed in the computational details and found to be the true minima on the potential energy surface characterized by the real values for frequencies. The energetic analysis suggests that **TDI** is relatively more stable than **TDI-1** by 6.2 kcal/mol (the calculated Boltzmann weighted population is 100 %).

The calculated ^{1}H (excluding labile protons) and ^{13}C NMR chemical shifts were correlated against the experimental values and the statistical parameters are presented in Table 3 and the correlation plots are shown in Figure 5. The complete chemical shift values are presented in Table S1 of supplementary material. From the correlations, it is observed that the correlation coefficient R^2 with respect to protons of **TDI** is 0.9641 which is close to unity compared to **TDI-1** (0.9204). The MAE, MaxE, CMAE and CMaxE of **TDI** (0.48, 1.48, 0.34 and 1.15) are relatively small compared to **TDI-1** (0.54, 3.17, 0.41 and 2.65). Similarly, the R^2 value with respect to carbons of **TDI** is 0.9956 which is close to unity compared to **TDI-1** (0.8589). Also, the statistical parameters of errors are small for **TDI** compared to **TDI-1** (Table 3). In addition, the formation of **TDI** is evidenced by the ^{13}C chemical shift value of C25 atom observed at 66.02 ppm and computationally at 70.96 ppm (Table S1) which is in line with the standard range of ~50-75 ppm for >CH–N (sp^3 carbon). This contrasts with the standard chemical shift range of ~145-160 ppm for CH=N sp^2 carbon (165.18 calculated, Table S1).[10] Taken collectively all the statistical correlations, the given experimental ^{1}H and ^{13}C NMR chemical shifts support to the proposed chemical structure of **TDI**.

Table 3. Relative energies (kcal/mole) and statistical parameters for the correlations of ^{1}H and ^{13}C NMR chemical shifts of **TDI** and **TDI-1** obtained at the B3LYP/6-31+G(d,p)//B3LYP/6-31+G(d,p) in DMSO solvent

Molecule	Relative Energy	R^2	MAE	MaxE	CMAE	CMaxE
^{1}H NMR						
TDI	0.0	0.9641	0.48	1.48	0.34	1.15
TDI-1	6.2	0.9204	0.54	3.17	0.41	2.65
^{13}C NMR						
TDI	0.0	0.9956	2.27	15.08	2.2	11.82
TDI-1	6.2	0.8589	7.06	99.16	8.55	99.17

†R^2 is the correlation coefficient, MAE is the mean absolute error, CMAE is the corrected mean absolute error, MaxE is the maximum error and CMaxE is the corrected maximum error with respect to the linear fit.

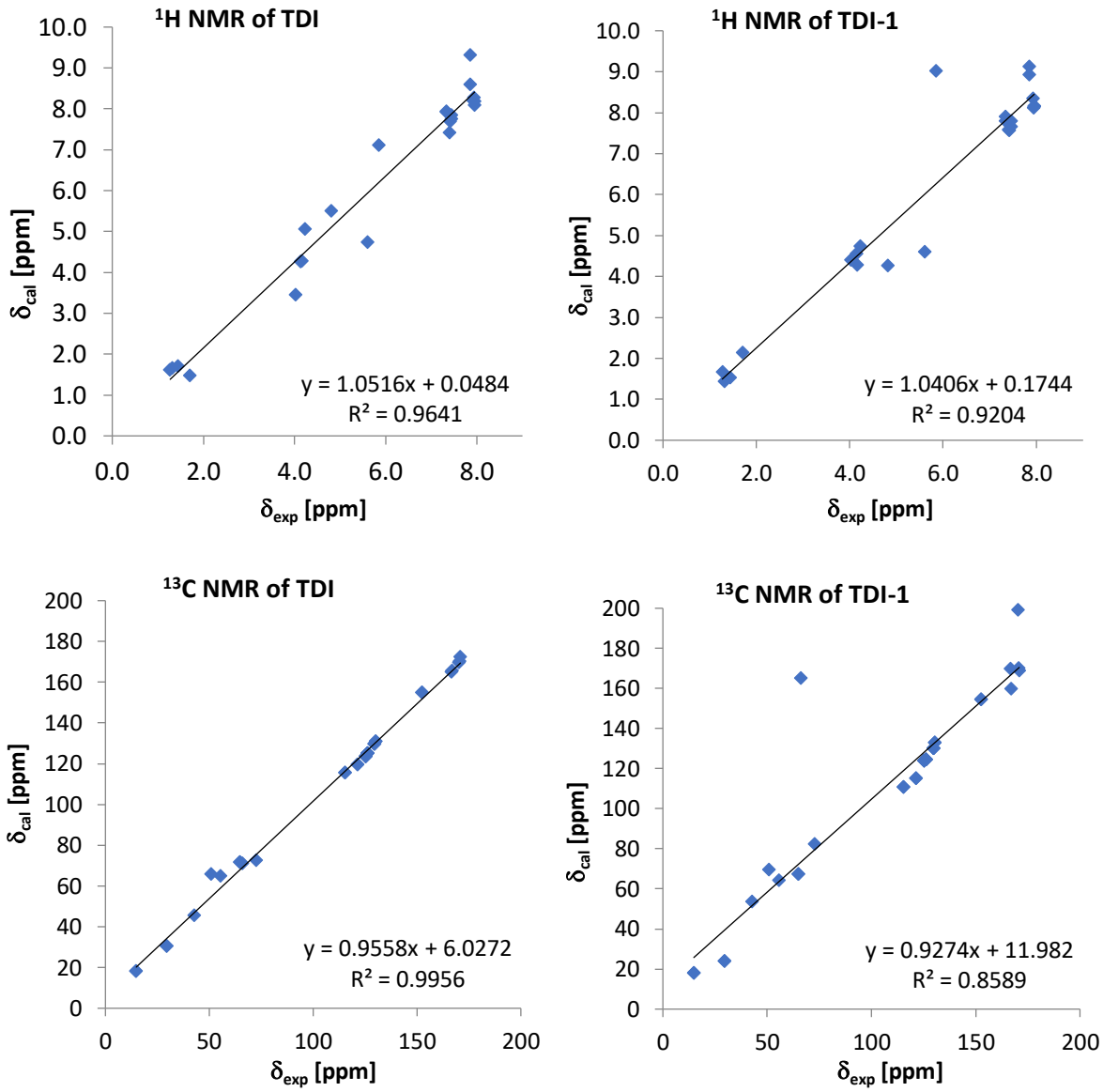

Figure 5. Correlation of simulated and experimental ^{1}H (top) and ^{13}C NMR (bottom) data of **TDI** and **TDI-1** obtained at the B3LYP/6-31+G(d,p)//B3LYP/6-31+G(d,p) level in DMSO solvent

IR structural characterization studies

The observed IR spectra of **TDI** showed a broad peak at 3600 to 2500 cm^{-1}, 3405.48 cm^{-1}, 1733.07 to 1515.11 cm^{-1} corresponding to O–H, N–H and C=O stretching's respectively. The presence of these functional groups confirms and validates the proposed structure of **TDI** (refer supplementary material for spectra). To support the observed values for the presence of these functional groups, computational simulations were performed at the same level. During the simulations, the vibrational wavenumbers are usually calculated using the simple harmonic oscillator model. Therefore, they are typically larger than the fundamentals observed experimentally and therefore the values are scaled with a scaling factor of 0.9648 as proposed by Merrick et. al. for this computational model.[11] The obtained values are presented in Table 4 and observed that the obtained values are within the range of the respective characteristic wavenumbers. This indeed supports the structure of **TDI**.

Table 4. Calculated harmonic wavenumbers (ν_{cal} cm^{-1}), relative infrared intensities (*A*, %), scaled harmonic wavenumbers (ν_{scal}, cm^{-1}) of TDI obtained at B3LYP/6-31+G(d,p) level of the theory along with the observed values IR values (ν_{obs}, cm^{-1}). The calculated values are scaled with 0.9648 scaling factor

Characterization	ν_{cal}	A	ν_{scal}	ν_{obs}	Vibration mode
ν(C14=O)	1707.48	355.67	1647	1733.07-1515.11	Stretching
ν(C17=O)	1714.83	220.55	1654		Stretching
ν(C20=O)	1801.23	207.96	1738		Stretching
ν(C27=O)	1813.03	414.98	1749		Stretching
ν(C30=O)	1729.5	171.66	1669		Stretching
ν(N15–H)	3587.64	117.45	3461	3405.48	Stretching
ν(N29–H)	3620.78	82.61	3493		Stretching
ν(O21–H)	3746	78.5	3614	3600-2500	Stretching
ν(O28–H)	3760.63	87.62	3628		Stretching

Mechanism of the Degradation Reaction

The proposed reaction mechanism for the formation of **TDI** is shown in Figure 6. The mechanism initiates by the hydrolytic ring opening of β-lactam in **NS** to obtain intermediate **NS-1** followed by the self-condensation to produce dimer, **NS2** which then undergoes elimination of 5,5-dimethyl-4,5-dihydrothiazole-4-carboxylic acid (DHTC) producing **TDI**.

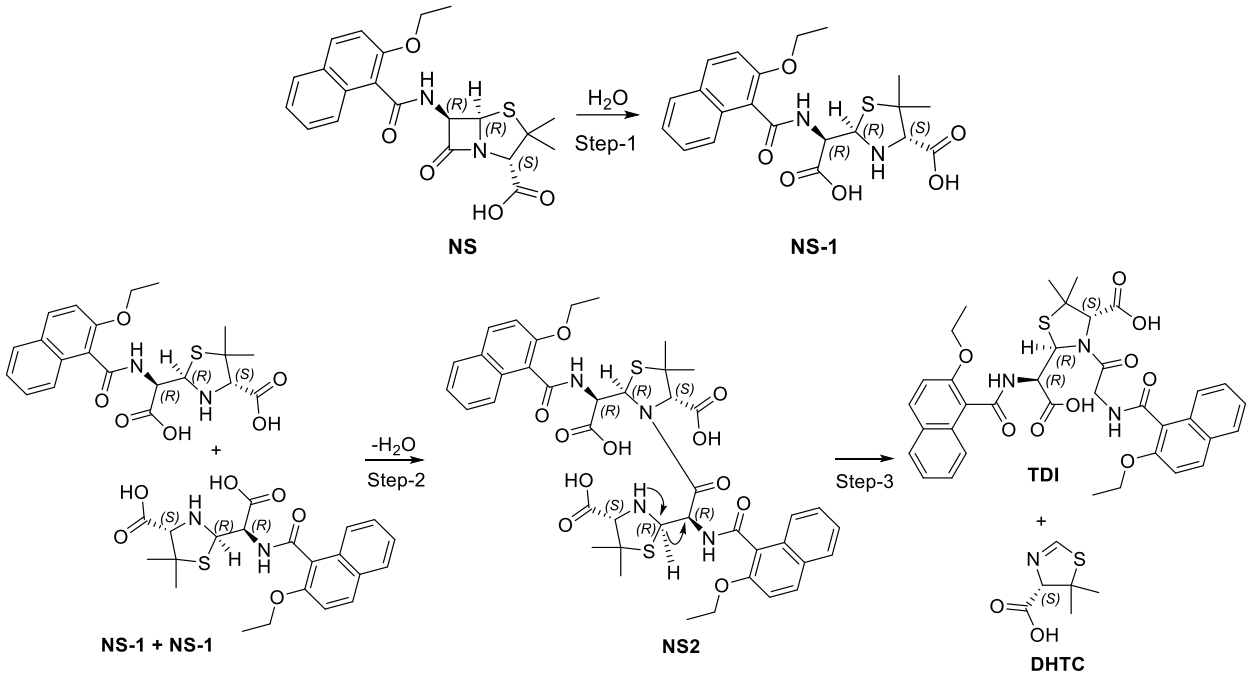

Figure 6. Proposed reaction mechanism for the formation of **TDI**.

Conclusions

The assessment of the novel degradation impurity of nafcillin sodium drug substance under thermal condition is presented. The impurity was isolated and fully characterized by various spectroscopic techniques like LC-MS, NMR and FTIR. Based on the spectroscopic data, probable structure for the degradation impurity is proposed. The proposed structure is further confirmed by the density functional calculations by predicting the NMR chemical shift values and performed statistical correlations against the available experimental data. In addition, a two-step mechanism of the degradation is proposed and involves the opening of the β-lactam followed by self-condensation. The present work will help the scientists and industry engaged in the method development and stability studies of Nafcillin.

Experimental Section

Chemicals and Reagents

NS sample was procured from RIA International (Hangzhou Dawn Ray Pharmaceutical make). HPLC grade solvents such as acetonitrile (ACN), n-hexane and isopropyl alcohol (IPA) and other chemicals such as ammonium acetate, glacial acetic acid (AcOH), hydrochloric acid (HCl), sodium hydroxide (NaOH), dichloromethane (DCM) and sodium chloride (NaCl) were purchased from Merck (Mumbai, India). HPLC grade purified water was obtained using a Milli-Q water purification system (Millipore Corporation, Billerica, MA, USA).

Instruments and instrumental parameters

Analytical high-performance liquid chromatography. A Waters Alliance HPLC (Waters Corporation, Milford, MA, USA) equipped with PDA detector was employed for the analysis of **TDI** and **NS**. The separation of **TDI** from **NS** was carried out using YMC ODS Aqua, 150 mm × 4.6 mm column packed with 5 µm particles. The flow rate

was 1.2 mL/min and the detection was carried out at 228 nm on a photodiode array (PDA) detector. The compounds were eluted with mobile phases having components A and B where A was 0.1% (v/v) formic acid in water while B was 100% ACN. A timed program of T/%B: 0/25, 40/65, 50/65, 51/25, 60/25 was followed for linear gradient.

Preparative high-performance liquid chromatography. A Waters preparative HPLC (Waters Corporation, Milford, MA, USA) equipped with UV-Vis detector was employed for the isolation of **TDI** using Cosmosil 5C18-MS-II, 250 mm × 20 mm column packed with 5 µm particles. The flow rate was 18 mL/min and the detection was carried out at 228 nm. The mobile phases consisted part A and B where part A was 0.1% (v/v) formic acid in water while B was 100% ACN. A timed program of T/%B: 0/40, 10/50, 21/50, 21.1/80, 23/80, 23.1/40, 28/40 was followed for linear gradient.

Liquid chromatography – Mass Spectrometry (LC-MS) LC-MS analysis was performed with Thermo Ion Trap Mass spectrometer (Thermo scientific, Waltham, MA, USA) coupled to an UHPLC quaternary gradient to study thermal degradation sample. Multi-stage fragmentation studies performed to evaluate the structures of **NS** and **TDI**. MS analysis was performed by applying Heated Electrospray Ionization (HESI) source in positive and negative ion modes. HESI source parameters setting involved source voltage 4.0 kV, capillary temperature 350°C, source heater temperature 350 °C, sheath gas flow 45.0, auxiliary gas flow 20.0, S-Lens RF level 60.0%. The data was acquired using Xcalibur software.

High resolution Mass Spectrometry (HRMS). HRMS analysis was carried out on SYNAPT G2 Q-TOF Mass spectrometer (Waters Corporation) coupled to an ACQUITY H-Class UPLC having quaternary gradient pump to identify the **NS** and **TDI** with accurate mass measurements. Q-TOF-MS/MS analysis was carried out to study the fragmentation patterns for **TDI** and **NS**. MS analysis was performed by applying electrospray ionization (ESI) source in positive ion mode. ESI source parameters setting involved capillary voltage 3.0 kV, source temperature 110 °C, desolvation temperature 250 °C, sampling cone 35 V, extraction cone 4.0 V, and desolvation gas flow 600 L/hour. Collision energy 18 eV was used for **TDI** to generate fragments. The data was acquired using Masslynx 4.1 software.

Nuclear Magnetic Resonance Spectroscopy (NMR). NMR spectral studies were carried out on Bruker Ascend 500, Avance III HD spectrometer (Bruker BioSpin AG, Industriestrasse 26, 8117 Fallanden, Switzerland) with Topspin software, version 3.2. Spectra were recorded using 500 MHz for ^{1}H NMR and 126 MHz for ^{13}C NMR at 298 K in DMSO-d_6 solvent. The chemical shift values were referenced to the tetramethylsilane (TMS) in DMSO-d_6. The proton and carbon chemical shift assignments were carried out with the help of two-dimensional (2D) correlation spectroscopy (COSY), total correlation spectroscopy (TOCSY), hetero nuclear single quantum correlation spectroscopy (HSQC), hetero nuclear multiple bond correlation spectroscopy (HMBC). All the experiments were carried out in the phase sensitive mode.[12] The spectra were acquired with 2×256 or 2×192 free induction decays (FID) containing 8–16 transients with relaxation delays of 1.0–1.5 sec. The 2D data were processed with Gaussian apodization in both the dimensions.

Fourier Transformed Infrared Spectroscopy (FTIR). The FT-IR spectra were recorded in the range of 4000 – 400 cm^{-1} using Perkin-Elmer Spectrum 100 spectrophotometer (Waltham, MA, USA). The sample pellet was prepared using dried KBr powder into a mortar with 1% of the sample.

Computational Details. All the calculations were performed using the Gaussian 09 program[13] with hybrid DFT-B3LYP functional[14] in conjunction with 6-31+G(d,p) basis set. This combination of the functional and basis set proved to provide accurate geometries and molecular properties for organic molecules at a reasonably low computational cost.[15] The gas phase molecular geometries of both **TDI** and **TDI-1** were energy minimized without any symmetry constraints and with the same stereo-configuration as in **NS**. The obtained geometries

were then subjected to the vibrational frequency analysis at the same Hessian to ensure that the obtained geometries represent minima on the potential energy surface.

The isotropic ^{1}H and ^{13}C NMR shielding constants were calculated by using the Gauge Independent Atomic Orbital (GIAO)[16] approximation. The equilibrium solvation effects were considered through an implicit solvation model for dimethylslufoxide (DMSO) by employing the self-consistent reaction field (SCRF) method in conjunction with the conductor-like polarizable continuum model (C-PCM).[17, 18] The chemical shifts were calculated as $\delta = \sigma_{ref} - \sigma$, where σ_{ref} is the shielding constant of the reference TMS calculated at the same level of theory (σ_{ref} = 31.6764 and 193.5149 respectively for ^{1}H and ^{13}C atoms).

To compare the calculated data with the experimental results, a linear fit of calculated versus experimental shifts ($\delta_{calc} = a + b\delta_{exp}$) is performed to obtain the intercept *a*, slope *b* and correlation coefficient R^2. The results were then evaluated in terms of mean absolute error, MAE = $\Sigma_n|\delta_{calc} - \delta_{exp}|/n$, the corrected mean absolute error CMAE = $\Sigma_n|\delta_{scaled} - \delta_{exp}|/n$, where $\delta_{scaled} = (\delta_{calc} - a)/b$ measures the distance between the experimental value and the value predicted by the linear fitting, the maximum error MaxE = max($|\delta_{calc} - \delta_{exp}|$) and the corrected maximum error CMaxE = max($|\delta_{scaled} - \delta_{exp}|$). It is noted that during the statistical analysis, the labile protons (NH and OH) are excluded from the correlation which would flatten all statistical parameters focusing on a narrower range allowed us to highlight the differences in the region of interest for the comparison. It is remarkable that the sources of variance in the calculated chemical shifts like conformational degrees of freedom in the ethoxy groups and flexibility of hydroxyl groups were neglected during the calculations.

Sample preparation

Degradation reaction and isolation of TDI. To a 250 ml single-neck round bottom flask equipped with magnetic stirrer was added 10 g (0.22 mol) of **NS** at room temperature (24-25 °C). The solid was heated to 105 °C and allowed to stir under nitrogen atmosphere. Degradation was monitored by HPLC and 13.21% product formation was observed after 88 hrs. Figure 7, top. The reaction was continued till 150 hrs, and no change in the percentage of product formation by HPLC is observed (Figure S1 of supplementary material). After completion of the reaction, 5 g crude solid was collected and dissolved in 60 mL of diluent (50% acetonitrile in water) for purification by preparative HPLC. A suitable preparative HPLC method was developed to separate and isolate **TDI** from residual drug substance and other impurities present in the mixture. The eluent (aq. acetonitrile) containing **TDI** was collected and solvent was evaporated. Solid compound was precipitated from the aqueous medium, filtered and dried at room temperature under vacuum. Weight of the resultant compound was about 170 mg which has 97.03% purity by HPLC, Figure 2, bottom.

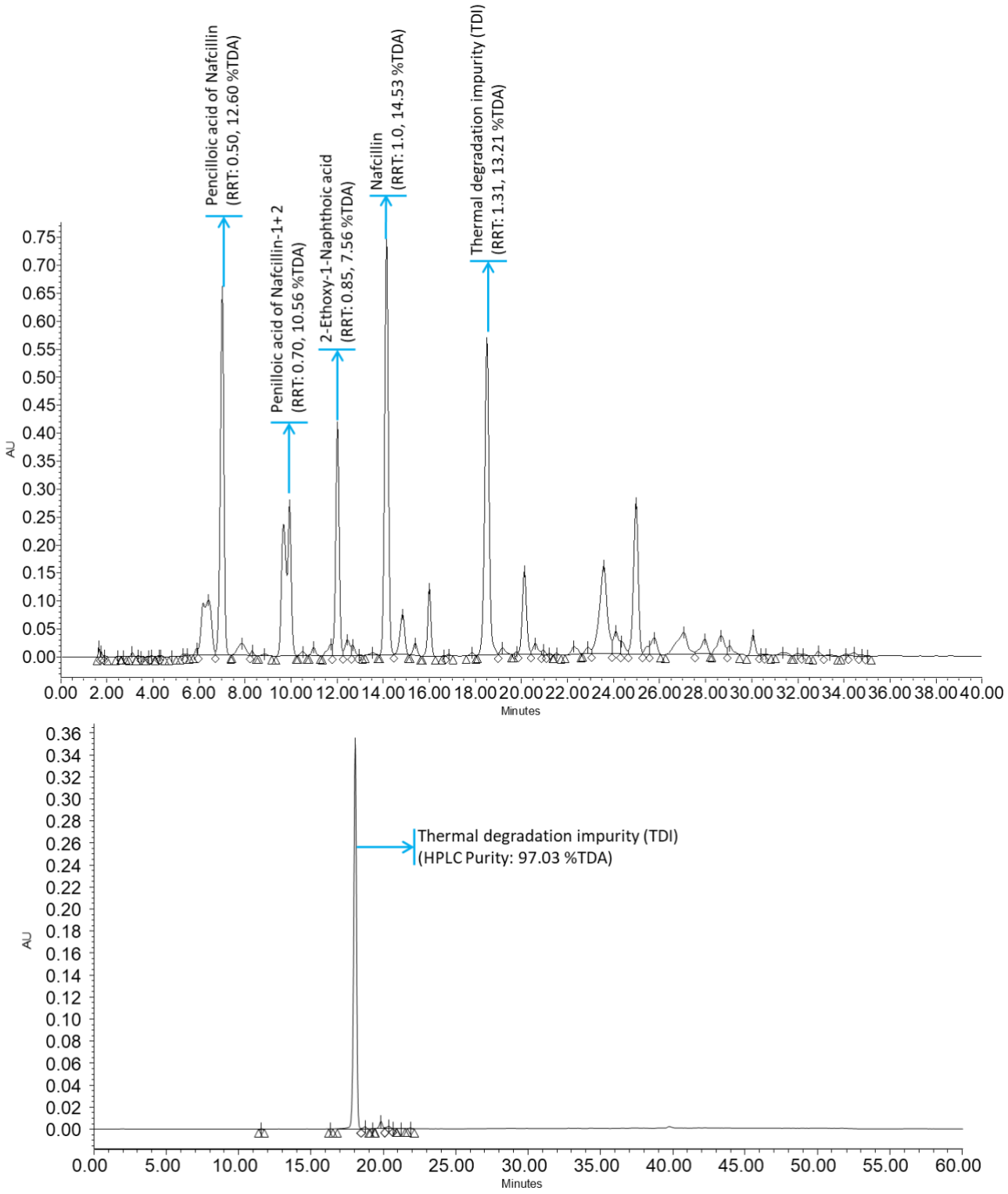

Figure 7. Crude HPLC chromatogram of **NS** obtained at 88 hrs. of thermal degradation (top) and chromatogram after purification (bottom).

Reverse phase achiral HPLC sample preparation. Weighed and transferred about 5 mg of **TDI** into a clean 10 mL volumetric flask. To this, 7 mL of diluent Acetonitrile was added and sonicated to dissolve. The volume of the solution was made up to the mark with diluent and mixed well.

Acknowledgements

The authors thank the management of United States Pharmacopeial Convention for permitting this work to be published.

Disclaimer: Certain commercial equipment, instruments, vendors, or materials may be identified in this paper to specify adequately the experimental procedure. Such identification does not imply approval, endorsement, or certification by USP of a particular brand or product, nor does it imply that the equipment, instrument, vendor, or material is necessarily the best available for the purpose or that any other brand or product was judged to be unsatisfactory or inadequate.

Supplementary Material

All the spectral data for the thermal degradation product (**TDI**) are provided in the Supplementary Material in the online version of the text.

References

1. Wade, K. C.; Benjamin, D. K., Chapter 37 - Clinical Pharmacology of Anti-Infective Drugs. In *Infectious Diseases of the Fetus and Newborn (Seventh Edition)*, Remington, J. S.; Klein, J. O.; Wilson, C. B.; Nizet, V.; Maldonado, Y. A., Eds. W.B. Saunders: Philadelphia, 2011; pp 1160. https://doi.org/10.1016/B978-1-4160-6400-8.00037-7
2. Ritter, J.; Flower, R.; Henderson, G.; Rang, H., Chapter 49 - Basic principles of antimicrobial chemotherapy. In *Rang & Dale's Pharmacology (Seventh Edition)*, Elsevier: Churchill Livingstone, 2011.
3. Vikhrova, N. M.; Strukov, I. T.; Tebiakina, A. E.; Chaikovskaia, S. M.; Shneerson, A. N.; Dubova, V. G. *Antibiotiki* **1965,** *10*, 3.
4. Bush, K., Chapter 14 - β-Lactam antibiotics: penicillins. In *Antibiotic and Chemotherapy (Ninth Edition)*, Finch, R. G.; Greenwood, D.; Norrby, S. R.; Whitley, R. J., Eds. W.B. Saunders: London, 2010; pp 200.
5. International Conference on Harmonization (ICH) of technical requirements for registration of pharmaceuticals for human use. ICH harmonized tripartite guideline. Stability testing of new drug substances and products, Q1A(R2), step 4 2003.
6. International Conference on Harmonization (ICH) of technical requirements for registration of pharmaceuticals for human use. Topic Q1B (R2): Photo stability testing of new drug substances and products, Geneva, 1996.
7. Blessy, M.; Patel, R. D.; Prajapati, P. N.; Agrawal, Y. K. *Journal of Pharmaceutical Analysis* **2014,** *4*, 159. https://doi.org/10.1016/j.jpha.2013.09.003
8. Rao, K. V. V. P.; Dandala, R.; Handa, V. K.; Rao, I. V. S.; Rani, A.; Naidu, A. *Arkivoc* **2006** (xv) 61. https://doi.org/10.3998/ark.5550190.0007.f08
9. Ashline, K. A.; Attrill, R. P.; Chess, E. K.; Clayton, J. P.; Cutmore, E. A.; Everett, J. R.; Nayler, J. H. C.; Pereira, D. E.; Smith, W. J.; Tyler, J. W.; Vieira, M. L.; Sabat, M. *J. Chem. Soc., Perkin Trans. 2* **1990**, 1559. https://doi.org/10.1039/p29900001559

10. Vundavilli, J. K.; Kothapalli, P. K. S. R.; Peruri, B. G.; Korrapati, P. R. V. V.; Sharma, H. K.; Nallapati, S. *Sci. Pharm.* **2015,** *83*, 95. https://doi.org/10.3797/scipharm.1408-03
11. Merrick, J. P.; Moran, D.; Radom, L. *J. Phys. Chem. A* **2007,** *111*, 11683. https://doi.org/10.1021/jp073974n
12. States, D. J.; Haberkorn, R. A.; Ruben, D. J. *J. Magn. Reson.* **1982,** *48*, 286. https://doi.org/10.1016/0022-2364(82)90279-7
13. Frisch, M. J.; Trucks, G. W.; Schlegel, H. B.; Scuseria, G. E.; Robb, M. A.; Cheeseman, J. R.; Scalmani, G.; Barone, V.; Petersson, G. A.; Nakatsuji, H.; Li, X.; Caricato, M.; Marenich, A.; Bloino, J.; Janesko, B. G.; Gomperts, R.; Mennucci, B.; Hratchian, H. P.; Ortiz, J. V.; Izmaylov, A. F.; Sonnenberg, J. L.; Williams-Young, D.; Ding, F.; Lipparini, F.; Egidi, F.; Goings, J.; Peng, B.; Petrone, A.; Henderson, T.; Ranasinghe, D.; Zakrzewski, V. G.; Gao, J.; Rega, N.; Zheng, G.; Liang, W.; Hada, M.; Ehara, M.; Toyota, K.; Fukuda, R.; Hasegawa, J.; Ishida, M.; Nakajima, T.; Honda, Y.; Kitao, O.; Nakai, H.; Vreven, T.; Throssell, K.; J. A. Montgomery, J.; Peralta, J. E.; Ogliaro, F.; Bearpark, M.; Heyd, J. J.; Brothers, E.; Kudin, K. N.; Staroverov, V. N.; Keith, T.; Kobayashi, R.; Normand, J.; Raghavachari, K.; Rendell, A.; Burant, J. C.; Iyengar, S. S.; Tomasi, J.; Cossi, M.; Millam, J. M.; Klene, M.; Adamo, C.; Cammi, R.; Ochterski, J. W.; Martin, R. L.; Morokuma, K.; Farkas, O.; Foresman, J. B.; Fox, D. J. *Gaussian 09, C.01*, Gaussian Inc., Wallingford CT: 2010.
14. Becke, A. D. *J. Chem. Phys.* **1993,** *98*, 5648. https://doi.org/10.1063/1.464913
15. Tirado-Rives, J.; Jorgensen, W. L. *J. Chem. Theory Comput.* **2008,** *4*, 297. https://doi.org/10.1021/ct700248k
16. Ditchfield, R. *Mol. Phys.* **1974,** *27*, 789. https://doi.org/10.1080/00268977400100711
17. Miertuš, S.; Scrocco, E.; Tomasi, J. *Chem. Phys.* **1981,** *55*, 117. https://doi.org/10.1016/0301-0104(81)85090-2
18. Barone, V.; Cossi, M. *J. Phys. Chem. A* **1998,** *102*, 1995. https://doi.org/10.1021/jp9716997